ARASHI SCIENTIFIC PUBLISHERS

Arashi Journal of Metals & Material Sciences
Volume 1, Issue 1 (Jul-Dec) 2024, pp. 47–57
DOI: 10.54646/jmms.2024.0007
www.asp-jmms.com

ORIGINAL RESEARCH

Polycaprolactone nanoformulated photosensitizer for photodynamic therapy

Koyeli Girigoswami[1] and Agnishwar Girigoswami[2]*

[1]Centre for Global Health Research, Saveetha Medical College, Saveetha Institute of Medical and Technical Sciences, Chennai, India
[2]Medical Bionanotechnology, Faculty of Allied Health Sciences, Chettinad Hospital and Research Institute (CHRI), Chettinad Academy of Research & Education (CARE), Chettinad Health City, Chennai, India

***Correspondence:**
Agnishwar Girigoswami,
agnishwarg@gmail.com;
dragnishwar@care.edu.in

Received: 15 February 2025; **Accepted:** 03 March 2025; **Published:** 07 March 2025

சுருக்கம்:
பல மருந்துகளுக்கு எதிர்ப்புத் திறன் (MDR) கொண்ட பாக்டீரியாக்கள் மிக ஆபத்தானவை. இவை பல்வேறு நோய்களை ஏற்படுத்த முடியும், சில நேரங்களில் மரணத்திற்கும் காரணமாக அமையும். MDR-ஐ கட்டுப்படுத்த பல சிகிச்சை முறைகள் இருந்தாலும், இந்த பாக்டீரியாக்களின் வேகமான வளர்ச்சி மனிதர்களுக்கு பெரும் சுகாதார ஆபத்தை ஏற்படுத்துகிறது. போட்டோடைனாமிக் தெரபி (PDT) என்பது ஒரு சிகிச்சை முறையாகும். இதில் போட்டோசென்சடைசர் ஒர் குறிப்பிட்ட அலைநீளத்தில் ஒளி படும்போது தூண்டப்பட்டு, ரியாக்டிவ் ஆக்ஸிஜன் ஸ்பீசிஸ் (ROS) உருவாக்குகிறது. இந்த முறையை தற்போது புற்றுநோய் மற்றும் MDR பாக்டீரியாக்களை அழிக்க பயன்படுத்துகின்றனர். இந்த ஆய்வில், ரோடமைன் 6G என்ற போட்டோசென்சடைசர், பாலிகாப்ரோலாக்டோன் (PCL) மற்றும் பாலிவினைலமைன் (PVA) மேட்ரிக்ஸ்-ல் என்காப்ஸுலேஷன் செய்யப்பட்டு அதன் பண்புகள் ஆய்வு செய்யப்பட்டது. இதைச் சரிபார்ப்பதற்காக DLS, zeta potential, FTIR, SEM போன்ற கருவிகள் பயன்படுத்தப்பட்டன. மேலும், ஐயோடைடு முறையின் மூலம் போட்டோசென்சடைசர்-ன் குவாண்டம் யீல்டு கணக்கிடப்பட்டது. போட்டோசென்சடைசர்-ன் பாக்டீரியா அழிக்கும் திறன் (PDT முறையில்) *E. coli* மீது பரிசோதிக்கப்பட்டது. முடிவில், போட்டோசென்சடைசர் வெற்றிகரமாக PCL-PVA மேட்ரிக்ஸ்-ல் என்காப்ஸுலேஷன் செய்யப்பட்டதாகவும், அதன் குவாண்டம் யீல்டு அதிகரித்ததாகவும் கண்டறியப்பட்டது. மேலும், 4 மணி நேர ஒளிச்சிகிச்சையின் பின்னர், 75% *E. coli* அழிப்பு ஏற்பட்டது. இந்த புதிய போட்டோசென்சடைசர், அதிக அளவு ROS உருவாக்கி MDR-யை எதிர்த்துப் போராட உதவக்கூடும். எதிர்காலத்தில், MDR-யை அழிக்க இது ஒரு புதிய சிகிச்சை முறையாக பயன்படலாம்.

Abstract:
Multidrug-resistant bacteria are the most vindictive microorganisms that can cause different disease manifestations, even leading to death. Despite many treatment strategies being present for combating multi drug resistance (MDR), the extensive proliferation of these bacteria is causing serious health threats for humans. Photodynamic therapy (PDT) is a treatment method in which a photosensitizer (PS) is excited to produce localized reactive oxygen species (ROS) after irradiation with light of a particular wavelength. This is nowadays used for the treatment of cancer as well as MDR killing. In this work, the PS, Rhodamine 6 G (R6G), was encapsulated in polycaprolactone (PCL) and polyvinylamine (PVA) matrix, and its characterization was done using different photophysical tools like DLS, zeta potential, FTIR, and scanning electron microscopy imaging. Further, the quantum yield of the engineered PS was calculated using the iodide method, and the quantum yield was estimated. Finally, the PS-induced killing of bacteria, *E. coli,* was assessed using PDT. The results indicated that the PS was successfully encapsulated in the PCL-PVA matrix, and the quantum yield was significantly enhanced. The encapsulated PS could also effectively inhibit the growth of *E. coli* and with 4 h irradiation time, a 75% bacterial cell killing was observed. The capacity of the encapsulated photosensitizer to produce ROS with high quantum yield has been demonstrated extensively. In the future, this novel photosensitizer may be used to kill MDR.

Keywords: photodynamic therapy, multidrug-resistant bacteria, photosensitizer, polycaprolactone, quantum yield

Introduction

Innumerable bacterial strains have turned antibiotic-resistant, i.e., the ability to put up with many antibiotics and chemotherapeutic drugs. This is termed as multi drug resistance (MDR) (1). In recent years, MDR cases have widely increased due to the repeated usage of antimicrobial drugs. This caused the evolution of drug insensitivity among the microorganisms. Several bacterial species are insensitive to many medications commonly prescribed. Therefore, researchers are concentrating on alternative treatment protocols. Photodynamic therapy (PDT) is a promising technique in this category, where light-sensitive fluorophores play a major role in inactivating MDR microorganisms (2). PDT is a kind of treatment modality in which reactive oxygen species (ROS) are locally generated by means of a photosensitizer (PS), appropriate wavelength of light, and oxygen presence. It is an assuring approach to treat MDR illness (3). At present, many researchers are engaged in PDT technology. PDT aids in cellular toxicity selectively by photo-illuminating the especially localized PSs (4). To become an efficient PS, the quantum yield should be maximum to generate the maximum singlet oxygen necessary for PDT (5). Previous research studies reported a significant quantum yield decrease with increasing PS concentrations tested in multiple types of PSs. The reason behind this decline was explained as self-quenching effects and aggregation of the dyes that hindered the energy transfer efficiency from the PS's excited triplet state to the molecular oxygen. These results indicated that optimum dye concentration and circumventing dye aggregation can ensure optimum efficacy of the PS in PDT (6, 7).

A capable alternative antimicrobial approach is PDT to battle against MDR bacterial contaminations (8, 9). Distinct from antibiotics, PDT is based on the principle of physical and chemical mechanisms that inhibit the development of resistance, cause the biofilm to break down, and work synergistically with antibiotics. This therapeutic modality can become a powerful means to fight against the superbugs. A photodynamic effect has been found to enhance innate immunity and eliminate bacteria by adoptively transferring macrophages loaded with near-infrared PSs (Lyso700D) (9). For the effectiveness of this therapy, future research is needed, and clinical trials can improve its medical application. PDT is effective against Gram-positive and Gram-negative bacteria and has been successfully used to treat MDR bacterial infections in diabetic ulcers (10) and chronic wounds (11) along with gentamicin, and burns (12, 13). PDT, in combination with photothermal therapy (PTT), has shown synergistic effects against these bacteria (14). PDT can reduce bacterial load, promote tissue healing, and can be applied in lung infection treatment caused by MDR *Pseudomonas aeruginosa* and *Klebsiella pneumoniae*, which are very common in ventilator-associated pneumonia (15, 16). MDR bacteria-induced dental plaque and periodontitis can be managed with PDT, circumventing inflammation and leading to oral health improvement (17). MDR *E. coli* and other resistant pathogens related to urinary tract infections can be managed by employing PDT, plummeting the need for high-dose antibiotics (18).

Nanotechnology has been employed in biomedical science with promising applications for a range of diseases (19, 20). PDT can be used for targeted delivery, and its efficiency can be improved by amalgamating nanotechnology with PDT (21). The solubility of PS can be enhanced by conjugating inorganic or organic nanomaterials, which helps in increased accumulation near the target location (22). The chief conjugation strategy for the nanomaterials is encapsulation. Several nanocarriers can be used for PS encapsulation, such as polymeric micelles, liposomes, and polymeric nanoparticles (23). Polycaprolactone (PCL) belongs to a semi-crystalline, aliphatic polyester material type with a melting point of 60°C. PCL is being used for medical applications due to its biocompatibility, biodegradability, low glass transition temperature, and non-hazardous stability (24). Owing to its excellent chemical, biological, and physical properties, PCL is considered to have great encapsulation potential that can be explored in therapeutics to facilitate the controlled release of the drug molecule (25). PCL is being used in tissue engineering due to its slower degradation rate (26). The aspiration of this study involves the quantification of ROS generation efficiency of PS encapsulated with the PCL-nanoparticle (PCL-NPs). The PS used in this study is Rhodamine 6G (R6G), an antimicrobial PS. R6G was encapsulated within PCL-NPs using polyvinylamine (PVA) as an emulsifying agent. The study compares the quantum yield efficiency of the PS (R6G) and PCL-NPs encapsulated PS (R6G-PCL-NPs).

Materials and methods

Materials

Ammonium molybdate ($(NH_4)_6Mo_7O_{24}$), disodium hydrogen phosphate (Na_2HPO_4), ethyl acetate ($C_4H_8O_2$), potassium iodide (KI), pyridine (C_5H_5N), Luria–Bertani (LB) broth were purchased from Sisco Research Laboratories Pvt. Ltd., PVA was obtained from Loba Chemie, India. PCL was obtained from Sigma Aldrich. Potassium dihydrogen phosphate (KH_2PO_4) was received from HiMedia, India.

Preparation of PCL nanoparticles

The PCL-NPs were prepared according to Ta et al. (27) with slight modifications. 100 mg of PCL was weighed in a test tube wrapped in aluminum foil, 1 ml of ethyl acetate was added to it, and the mouth was enclosed with

parafilm. High-speed vortexing for approximately 10 min was needed to dissolve the polymer fully. 0.3% PVA was dissolved in 47 ml water using a hot plate, and the fully dissolved PVA solution was stirred vigorously at 360 rpm for a further 10 min. 2 ml PVA solution was taken in the test tube, and PCL solution was added dropwise carefully. The solution was vortexed well for the emulsion to be formed for a further 30 min. The emulsified polymer was sonicated for three 10 s burst sonications (40% amplitude for a 700 W sonicator, 1/8 in probe tip size), keeping the test tube immersed in ice-cold water. 1–2 ml from the stirring PVA solution was added to the emulsified polymer. This step enables the emulsion to be diluted so that it can be easily poured into the stirring PVA solution. After merging both the solutions, the sides were wrapped with aluminum foil, leaving the top open. Solidification of the particles was enabled by 3 h stirring. After stirring, the solution was subjected to centrifugation for about 15 min at 14,000 rpm. The pellet was collected, diluted with 5 ml of distilled water, and stored at room temperature (28). **Figure 1** shows the scheme of preparation of the PCL-NPs.

Nanoparticles collection and characterization

After stirring, we split the polymer solution into two oak ridge centrifuge tubes. We centrifuge the polymer solution in a fixed angle rotor at 17000 rpm for 15 min. The supernatant was discarded, and 5 ml of distilled water was added to the pellet for further analysis. The characterizations of the synthesized nanoparticles were done using a particle size analyzer (Malvern zetasizer) and a UV-visible spectrophotometer (Shimadzu UV 1800). The characteristic bands of the synthesized R6G-PCL-NPs and PCL were recorded in transmittance mode using an FTIR (19). A KBr pellet was made, and the measurement was performed using a Bruker Alpha FTIR instrument. Surface morphological observation and knowledge about the nanosize of the synthesized R6G-PCL-NPs were done using scanning electron microscopy (SEM) (20). A thin layer of the R6G-PCL-NPs was drop cast on a grease-free clean glass coverslip and subjected to air drying in a closed container to avoid dust deposition. The R6G-PCL-NPs, layered onto the glass coverslip, were covered with a thin gold layer to enhance their conductivity prior to SEM imaging. 25 kV voltage was applied to get the SEM image using JSM-IT800 Nano SEM.

Encapsulation of R6G in PCL-NPs

The 5 µl of 0.9 mM R6G was added to 3 ml of PCL-NPs and kept in an ultrasonic bath sonicator for 15 min. After 15 min, the dye was encapsulated in the nanoparticle. The encapsulation efficiency (EE) was confirmed by centrifugation method (29). Initially, the OD of the encapsulated dye was measured at 529 nm using a Shimadzu UV1800 spectrophotometer. Further, the dye-encapsulated particle was centrifuged at 10,000 rpm using REMI RM-03 Plus microcentrifuge for 15 min. The supernatant was slowly aspirated from the tube, and the absorbance of the supernatant was taken at 529 nm. The EE was calculated using the following formula according to Pragya *et al.* (3).

$$\textit{Encapsulation efficiency (percent)} = \frac{(OD)\ \textit{initial} - (OD)\ \textit{supernatant}}{(OD)\ \textit{initial}}$$

Where (OD) initial is the absorbance of the initial amount of drug; (OD) supernatant is the absorbance of the supernatant.

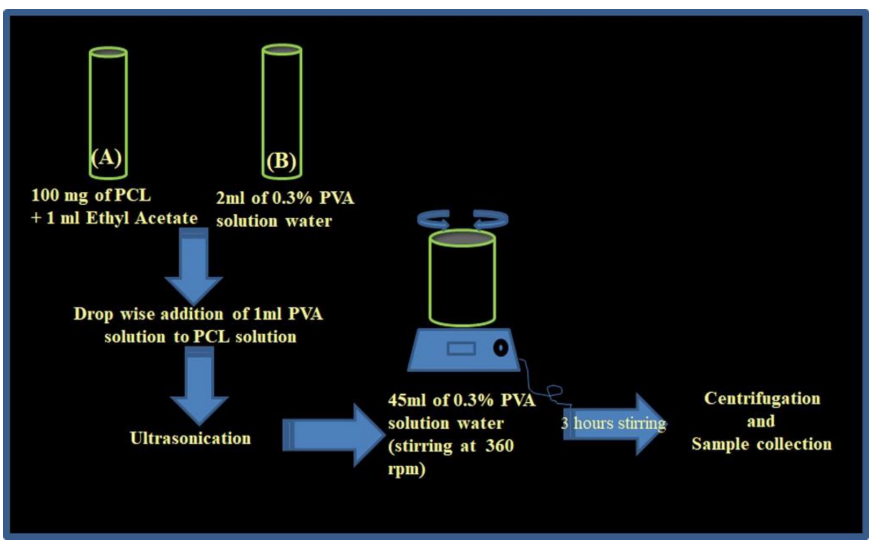

FIGURE 1 | Synthesis of PCL-NPs using single emulsion method.

Quantification of ROS generation using the iodide method

Whenever a sensitizer is excited with light $^1O_2$ is generated that can react with the iodide ions (I^-) if a catalyst, usually, $(NH_4)_2MoO_4$ is present (3). The outcome of the reaction yields I_3^-, whose production amount is directly proportional to the amount of $^1O_2$ produced (2, 30), which can be further measured using a spectrophotometer (Shimadzu UV-1800). The absorbance was recorded at 351 nm, keeping the OD values less than 0.1. The PS was solubilized in a reagent containing iodide and catalyst (potassium iodide (KI) 0.12 M, catalyst $(NH_4)_2MoO_4$ (10 mM) dissolved in Na-K phosphate buffer (0.05 M; pH = 6.2). The calculation of the quantum yield of I^- (F_{ox}) oxidation was done using the following equation that is adopted from the photooxidation theory:

$$F_{ox} = \frac{R_{ox}}{I_a} = \frac{F_D k_r [I^-]}{k_d + k_q [I^-]} = F_D P$$

Where, R_{ox} and I_a are the oxidation rate of I^- and the absorbed light intensity of the irradiated solution, respectively, k_r represents the chemical reaction rate constant of the I^- with $^1O_2$, k_q abbreviates the overall bimolecular rate constant for quenching of $^1O_2$ by I^-, k_d denotes the quenching rate constant of $^1O_2$by the solvent, F_D represents the quantum yield of $^1O_2$, P denotes the fraction of $^1O_2$chemically reacting with I^-.

In the presence of an incessant output of light source and a given absorbance capacity of PS at its excitation wavelength (λ_{max} = 529 nm), the OD change of the triiodide band ($A(I_3^-)$) with respect to time is directly proportionate to the oxidation rate of $I^-(R_{ox})$. Considering the PS absorbance as A, and according to the Lambert-Beer law, the $1 - 10^{-A}$ expression is proportionated in a direct manner to the PS's part of the radiation absorbed. When a graph is plotted between I_3^- absorbance at 352 nm with time, a straight line is observed, and the slope of that line is B. B is proportional to the product (I_3^-) formation or oxidation rate of I^-. A slope is obtained when B's dependence on $1 - 10^{-A}$ expression is plotted, which is represented as k, is eventually directly proportionate to the F_{ox} (relative quantum yield of the oxidation) and therefore also to the F_D. In this manner, the singlet oxygen quantum yield (SOQY) for R6G was estimated in the nanoformulation of R6G.

Experimental setup

Figure 2 represents the apparatus set up for the generation of ROS. The source of light used here was a xenon arc lamp, which works by the power source. It generates light of wavelength approximately around the 185–2000 nm range. The photodynamic light experiments require only 400–700 nm of light (i.e., the visible range). Thus, light should be filtered for that required range with the help of a UV+IR filter that consists of 1 cm of pyridine and 10 cm of potassium iodide solution. The light from the filter passes through the 1 cm glass cuvette in which the sample is placed. The sample comprises PS, which, on irradiation with light, generates the ROS.

Antimicrobial assay using engineered PS and *E. coli*

The bacterial growth inhibition was tested in *E. coli*. The bacteria were grown overnight in LB broth at 37°C in a shaker incubator in two sets. In both sets, the engineered PS (R6G-PCL-NPs) was added at a concentration of 300 nM, and in one set, the light exposure was given for four hours.

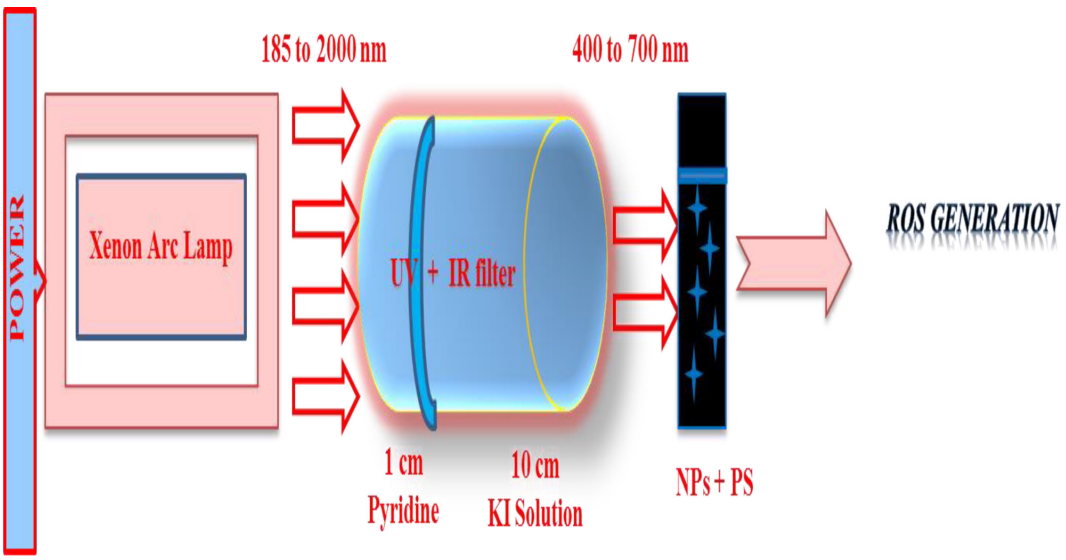

FIGURE 2 | The working setup of photodynamic light experiments.

Every 30 min, we aspirated the sample and measured the absorbance at 600 nm to monitor the effect of exposure to bacterial killing. The absorbance was measured for the other set under identical conditions, without light exposure, against only LB as a blank. The amount of bacterial growth is directly proportional to the OD at 600 nm (31).

Statistical analysis

Student's t-test was used to evaluate the level of significance. $p < 0.01$ was considered significant.

Results and discussion

Absorption spectra of R6G

The plot of OD versus wavelength (absorption spectra) of R6G showed that λ_{max} was at 529 nm with a small shoulder at 480 nm in water. The absorbance of R6G dissolved in water with variable concentration was plotted in **Figure 3a**. The OD was maintained at less than 0.1.

Characterization of PCL-NPs

PCL-NPs were prepared by the single emulsion method. Dynamic light scattering was used to record the hydrodynamic diameter and polydispersity index (PdI) of PCL-NPs. The PCL-NPs showed a PdI of 0.255, and the hydrodynamic diameter was 130 nm (**Figure 3b**). The mono-dispersity of the nanoparticles was noted due to a low polydispersity index (PdI). If the sample is not properly prepared for DLS or the measurement is not well-optimized, a size can still be reported. However, various artifacts may distort the data, resulting in uncertainty in the measured size. Among the two scattering peaks, the major peak was at 130 nm, which was attributed for the particle's hydrodynamic diameter (32, 33). The result was supported by the SEM data (**Figure 3c**), where the size of the particles was 110 nm. To identify the surface potential of the prepared particle, the zeta potential of the prepared PCL-NPs was measured, and it was found to be −24.2 mV, which ensures a high stability of the nanoparticles in water. The FTIR spectrum of PCL, which is partially crystalline, showed absorption bands corresponding to typical linear aliphatic polyester (**Figure 3d**). Double bands between 2800 and 3000 cm^{-1} represent the stretching of C—H bonds in the methylene groups, while a single peak at 1720–1730 cm^{-1} represents the presence of the carbonyl group. Additional peaks between 700 and 1600 cm^{-1} indicate the properties of the polymer's skeleton, including wagging, bending, and stretching of the constituent methylene groups, as well as isomerization of the ester groups (34, 35). On the other hand, the R6G-PCL-NPs exhibited a shift in the band of each wavenumber, indicating the PCL-NPs formulation. When a drug molecule is entrapped inside a polymeric structure, the different bonds are stretched or bent to accommodate the drug inside. In such a case, a few peaks may shift to a higher wavenumber and some towards a lower wavenumber. Since the property of the material is the same, all the peaks will be present corresponding to that of the encapsulating nanoparticle (36, 37). The SEM images display the surface morphology of the R6G-PCL-NPs. The shape is spherical and resembles a uniform distribution throughout the surface. The SEM image typically shows an egg box-like structure, as expected in polymeric nanoparticles. The diameter of the R6G-PCL-NPs, as revealed by SEM analysis, was 110 nm. Similar nanometer-sized PCL-NPs have been reported by earlier researchers (38).

Efficiency of ROS generation

The reactive O_2 generation was estimated using the iodide method. Aqueous R6G in the iodide reagent and R6G-PCL-NPs in the iodide reagent were used to compute the ROS quantum yield. The EE was found to be 62%, and the concentration of R6G was 300 nM. Light exposure was given to the samples in the presence of potassium iodide and ammonium molybdate. The O_2 generated by the light, in the presence of the catalyst ($(NH_4)_6Mo_7O_{24}$) can react with I^- for I_3 generation. I_3 generation is dependent on the irradiation time at different PS concentrations, which was measured spectrophotometrically at 351 nm. The optical density of R6G at 529 nm (the wavelength for excitation (λ_{ex}) of R6G) was selected randomly, keeping the absorbance value less than 0.1. The band for triiodide depended on the time of irradiation for the solution with flexible R6G concentration in the iodide reagent (**Figure 4**). We have fitted the experimental points in a straight-line fitting for each iodide reagent concentration in R6G. For each straight line, eventually, the slope B and the correlation coefficient, including the standard deviation, were estimated for individual straight lines. All the B values were calculated with the correlation coefficient corresponding to linear regression. As the B value was related to the triiodide formation, we plotted the B values against $1 - 10^{-A}$. Linear regression was used to fit the data points to a straight line. The resulting linear relationship that gave a straight line passing through the origin indicated no shielding effect existed or no complex photooxidation mechanism was present. The slope of the plot (k) was taken to calculate the quantum yield of R6G in water by associating it with the standard values for H2TPPS4 ($k = 730 \times 10^{-5}$ s^{-1} and $\Phi = 0.62$). Consequently, the SOQY of R6G in water was found to be 0.39. (**Figure 5**).

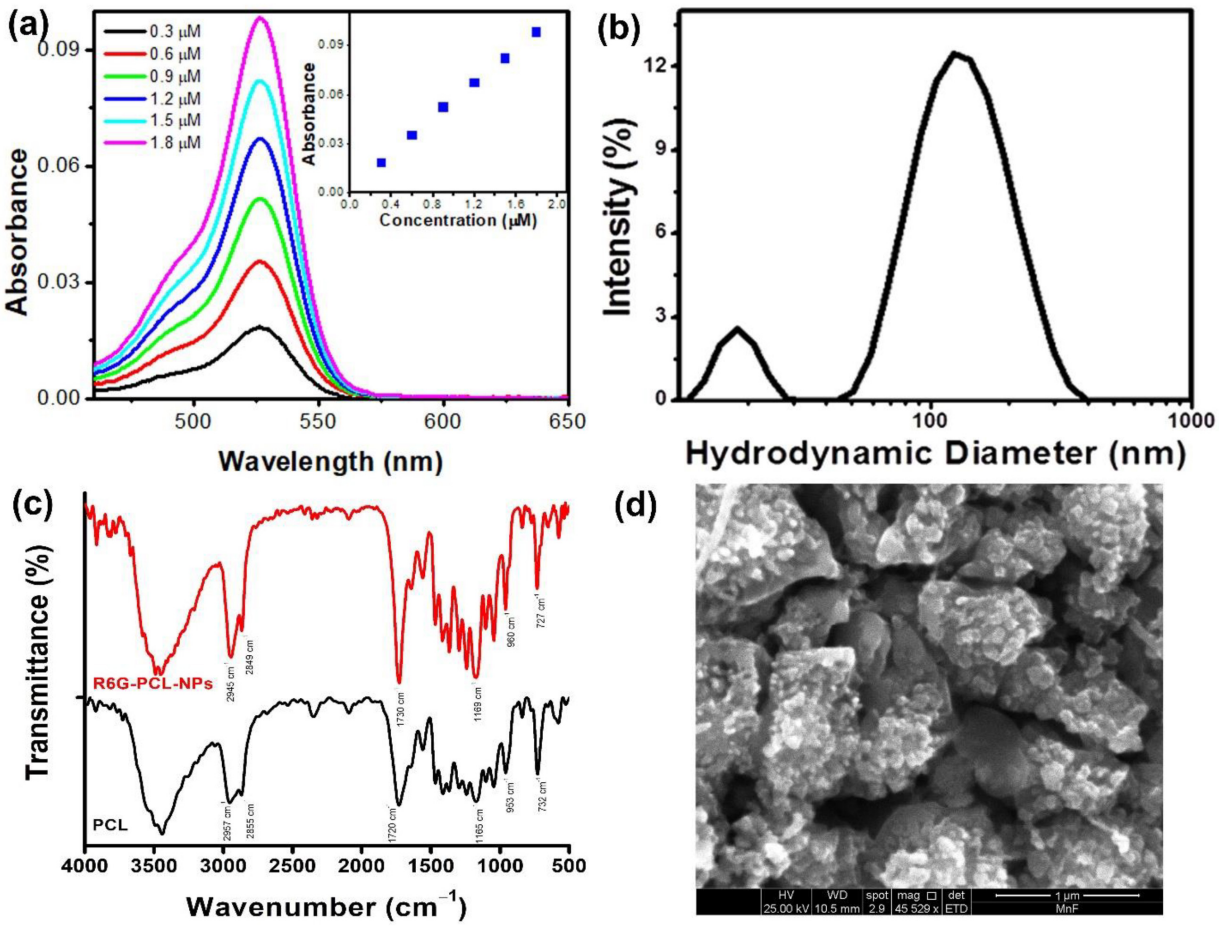

FIGURE 3 | (a) Absorption spectra of R6G in water with varying concentrations. **(b)** DLS image showing the hydrodynamic diameter of the prepared PCL-NPs. **(c)** The FTIR spectra of PCL and R6G-PCL-NPs. **(d)** The SEM image of R6G-PCL-NPs.

Quantification of ROS generation for R6G-PCL-NPs

Similar experiments were carried out after encapsulating R6G in PCL-NPs (R6G-PCL-NPs), and an estimation of the SOQY was made (**Figure 6**). The SOQY is 0.85 for R6G-PCL-NPs. This value was found to be higher compared to aqueous R6G, which indicated that this encapsulated R6G had a higher capacity to generate singlet oxygen. It is known that high photoactivity is seen in the case of monomeric dyes, and the production of singlet oxygen of a PS is heavily influenced by dye aggregation (5). The high SOQY of R6G-PCL-NPs confirms the monomerization of R6G in nanoformulation.

Antibacterial activity exhibited by R6G-PCL-NPs through PDT

The antibacterial effect of the designed PS post-exposure to light was demonstrated in Gram-negative bacteria *E. coli*. **Figure 7** shows the growth inhibition of the bacteria. The PDT setup is shown in **Figure 7a**, which clearly shows that the light source is monochromous. **Figure 7b** and **c** shows the growth of bacteria before and after exposure to light. In tube 1, only LB is present; in tube 2, bacteria with R6G-PCL-NPs are present; and in tube 3, bacteria with R6G-PCL-NPs are present, which was subsequently exposed to light. Visible clearance of bacteria is observed in tube 3 of **Figure 7c**, which is also supported by the quantitative evidence depicted in **Figure 7d**. In **Figure 7d**, there was a significant difference in bacterial OD after 90 min of exposure up to 240 min between the irradiated sample compared to the non-irradiated one. This drastic decrease in bacterial absorbance at 600 nm indicated that the PS was having a considerable bactericidal effect. After 4 h of irradiation in the presence of the encapsulated PS, the killing rate was 75%.

The results of this experiment with bacteria demonstrated that the PS alone does not kill the bacteria, but in the presence of light, it can kill them. Similar studies have been reported for killing bacteria (39) as well as cancer cells (3) by other investigators.

Infections caused by multidrug-resistant bacteria (MDR bacteria) are difficult to treat because they are resistant to multiple antibiotics. In addition to prolonging illnesses, increasing medical costs, and increasing mortality rates, these bacteria are highly dangerous to public health

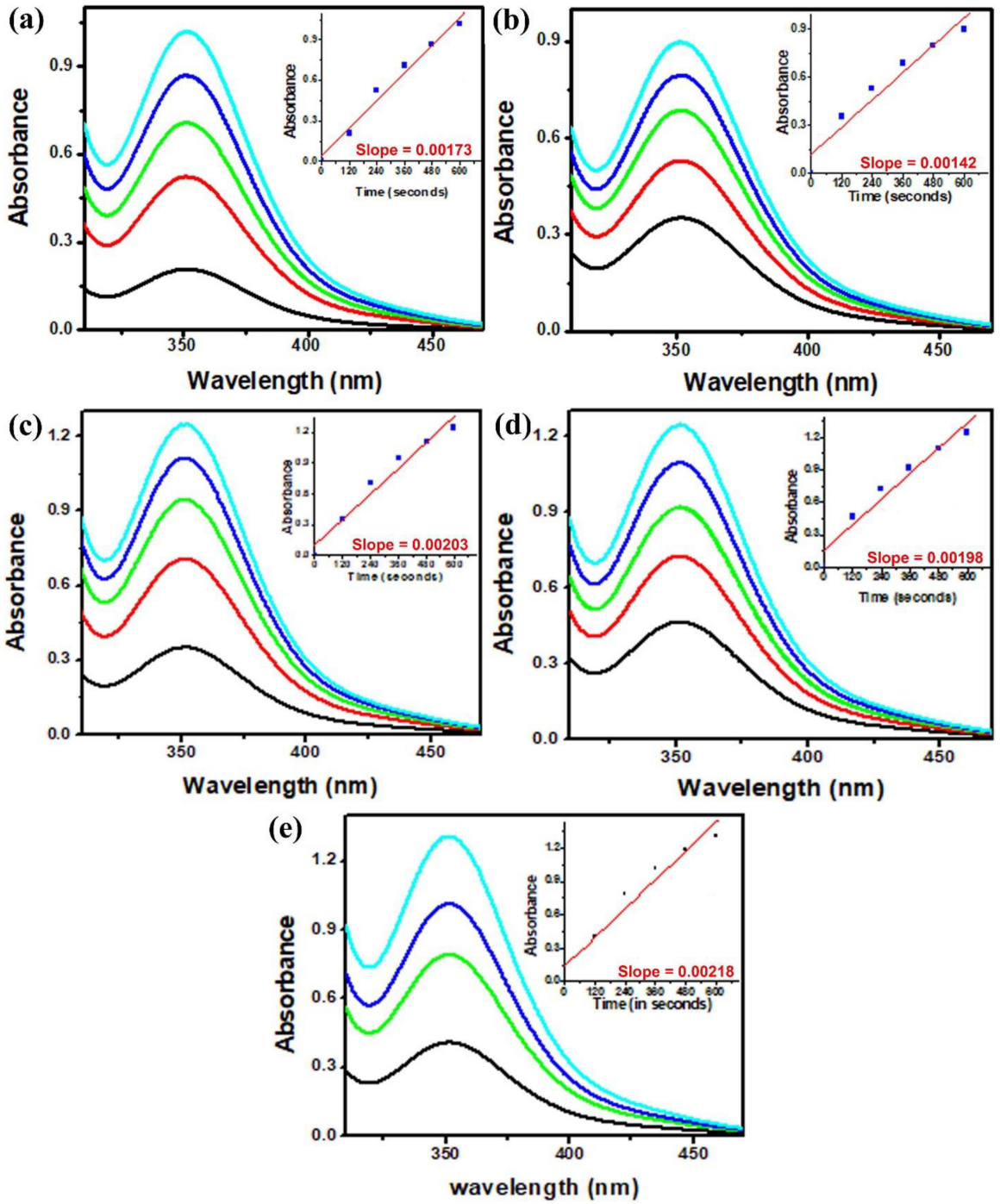

FIGURE 4 | The absorbance of the triiodide band was dependent on the irradiation time as shown in **(a)** 3 μM, **(b)** 6 μM, **(c)** 9 μM, **(d)** 12 μM, and **(e)** 15 μM of R6G.

(40). Several factors contribute to the development of multidrug resistance, including overuse, misuse, incomplete antibiotic courses, insufficient infection control, and frequent antibiotic use in hospitals (41). It is also possible that antibiotic resistance spreads to humans via food and the environment when antibiotics are used in livestock. There are some types of MDR bacteria, but methicillin-resistant *Staphylococcus aureus* (MRSA) is the most common and can manifest pneumonia and infection in blood and skin (42). There are also MDR strains of bacteria, such as Vancomycin-resistant *Enterococcus* (VRE), that are responsible for infection of the urinary tract and bloodstream (43). Hospital-acquired infections are caused predominantly by Carbapenem-resistant *Enterobacteriaceae* (CRE) (44) and Multidrug-resistant *Pseudomonas aeruginosa* (45). Patients with critically ill conditions may be susceptible to multidrug-resistant *Acinetobacter baumannii*, which may cause wound infections and pneumonia (46). Healthcare

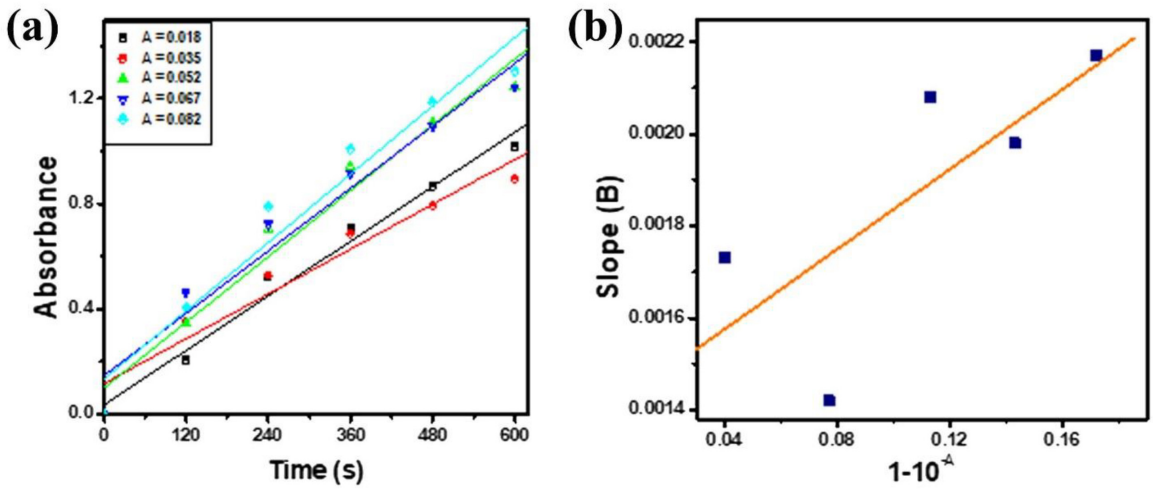

FIGURE 5 | (a) The dependence of the absorbance of the triiodide band for variable concentrations of R6G on irradiation time. **(b)** Association between the slope B and the fraction of light ($1 - 10^{-A}$) absorbed by R6G for different concentrations of the iodide reagent. The quantum yield (Φ) was found by the iodide method to be 0.39.

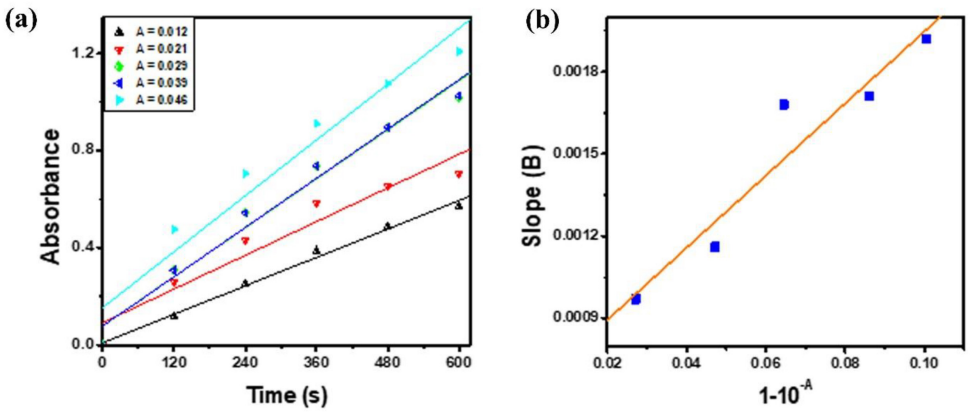

FIGURE 6 | (a) Relationship between the absorbance of the triiodide band with variable concentrations of R6G-PCL-NPs on irradiation time. **(b)** Association between slope B and the light fraction ($1 - 10^{-A}$) absorbed by R6G-PCL-NPs for different iodide reagent concentrations. The quantum yield (Φ) was found by the iodide method to be 0.85.

systems are burdened by multidrug-resistant bacteria due to longer hospital stays, higher treatment costs, and outbreak risk. The evolution of bacteria has warranted the need for new therapeutic approaches like antimicrobial peptides, phage-based therapy, and PDT. In this study, we have developed a specific PS that was used to kill the microbes via PDT.

PCL-NPs were prepared using a single emulsion method and characterized using DLS and zeta sizer. The solution of Rhodamine-6G was prepared, and the absorption peak was observed at 529 nm using a UV-vis spectrophotometer. The Rhodamine-6G was encapsulated within the PCL-NPs to evaluate the ROS quantum yield, and the EE was 62%. For the quantification of ROS generation efficiency of both R6G and R6G-PCL-NPs, the iodide method was employed using the photodynamic setup and UV- vis spectrophotometer. Finally, the quantum yield was calculated, and the ROS-generating property was found to be higher in the case of R6G-PCL-NPs. A step forward, the engineered PS was effective in killing the Gram-negative bacteria, *E. coli*, after exposure to light, demonstrating its PDT capacity. Hence, it can be indicated that R6G-PCL-NPs have better abilities to photodynamically inactivate microbes by generating singlet oxygen species. In combination with antibiotics, PDT can enhance the killing of bacteria (47).

Although PDT is very promising, there are several challenges that hinder its efficient application (48). First is the distribution of the PS inside the body, which can be uneven and can reach non-target regions, causing unwanted damage. Secondly, the penetration power of the light is very shallow, and there is a significant attenuation of the light as it passes through the tissues. Thirdly, under hypoxic conditions, PDT cannot be used since the PSs cannot generate singlet oxygen (49, 50). Several nanotechnological approaches have been

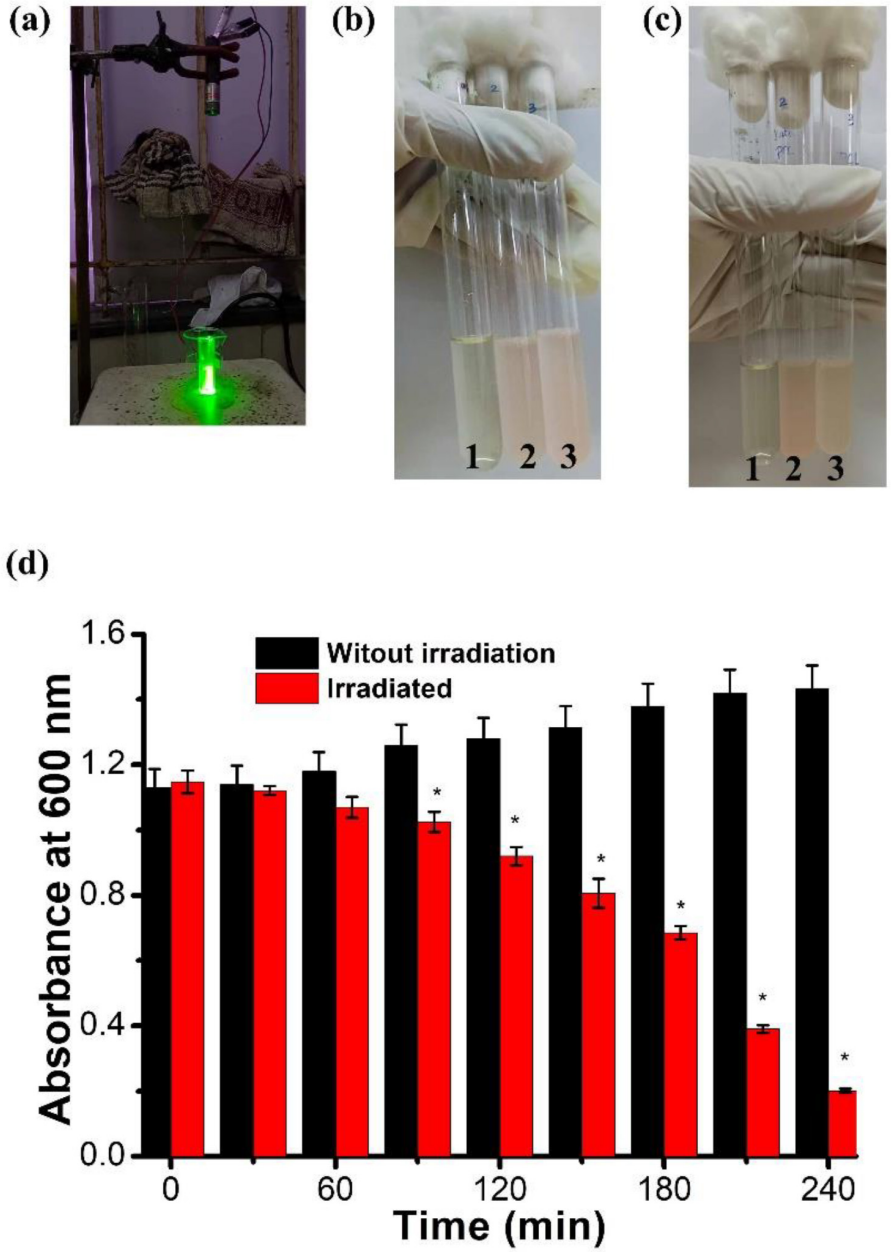

FIGURE 7 | The bactericidal activity for the R6G-PCL-NPs was measured using PDT. **(a)** The PDT set up using the laser light **(b)** The tubes containing only LB (1), *E. coli* in LB plus PS (2 and 3) before irradiation. **(c)** The tubes containing LB (1), *E. coli* in LB plus PS (2), and *E. coli* in LB plus PS after 2 h irradiation (3). **(d)** The absorbance at 600 nm at different time intervals for unirradiated bacteria (black) and irradiated bacteria (red) (* represents a significant difference at $p < 0.01$).

identified to improve the efficacy of PDT, and future research is warranted to overcome these limitations.

Conclusion

PCL-NPs were prepared using a single emulsion method and characterized using DLS and zeta sizer. The solution of Rhodamine-6G was prepared, and the absorption peak was observed at 529 nm using a UV-vis spectrophotometer. The Rhodamine-6G was encapsulated within the PCL-NPs, with an encapsulation efficiency of 62%, to evaluate the ROS quantum yield. For quantification of ROS generation efficiency of both R6G and R6G-PCL-NPs, the iodide method was employed using the photodynamic setup and UV-vis spectrophotometer. Finally, the quantum yield was calculated, and the ROS-generating property was found to be higher in the case of R6G-PCL-NPs. Antimicrobial assessment was done using PDT and *E. coli*. It was found that with only our engineered PS, there was no killing observed, whereas with PS and green light exposure for 2 h, a significant amount of killing was observed. Hence, it can be indicated

that R6G-PCL-NPs has better abilities to photodynamically inactivate microbes by generating singlet oxygen species, and the killing was 75% after 4 h of irradiation. In combination with antibiotics, PDT can enhance bacterial killing. The present investigation has revealed an engineered PS which exhibits an enhanced quantum yield. This can be effectively used in the future for the design of PSs that can kill MDR bacteria. The limitations of PDT include limited penetration of light to the target site, selection of proper PSs, and dose optimization when used in combination with antibiotics and immunotherapy.

Conflicts of interest

The authors declare no conflicts of interest.

Acknowledgement

We are grateful to Chettinad Academy of Research and Education for supporting the study.

References

1. Jacopin E, Lehtinen S, Débarre F, Blanquart F. Factors favouring the evolution of multidrug resistance in bacteria. *J R Soc Interf.* (2020). 17:20200105.
2. Pallavi P, Sharmiladevi P, Haribabu V, Girigoswami K, Girigoswami AA. Nano approach to formulate photosensitizers for photodynamic therapy. *Curr Nanosci.* (2022) 18:675–89.
3. Pallavi P, Harini K, Crowder S, Ghosh D, Gowtham P, Girigoswami K, et al. Rhodamine-conjugated anti-stokes gold nanoparticles with higher ROS quantum yield as theranostic probe to arrest cancer and MDR bacteria. *Appl Biochem Biotechnol.* (2023) 195:6979–93.
4. Pallavi P, Harini K, Mahata A, Thirumalai A, Girigoswami K, Girigoswami A. Revolutionizing cancer treatment through nanoengineered photosensitizer formulations for advanced photodynamic therapy. *Int J Nano Dimen.* (2024) 15:1–27.
5. Ji C, Lai L, Li P, Wu Z, Cheng W, Yin M. Organic dye assemblies with aggregation-induced photophysical changes and their bio-applications. *Aggregate.* (2021) 2:e39.
6. Szewczyk G, Mokrzyński K. Concentration-dependent photoproduction of singlet oxygen by common photosensitizers. *Molecules.* (2025) 30:1130.
7. Tanielian C, Heinrich G. Effect of aggregation on the hematoporphyrin-sensitized production of singlet molecular oxygen. *Photochem Photobiol.* (1995) 61:131–5.
8. Jia Q, Song Q, Li P, Huang W. Rejuvenated photodynamic therapy for bacterial infections. *Adv Healthcare Mater.* (2019) 8:1900608.
9. Wang Z, Wu A, Cheng W, Li Y, Li D, Wang L, et al. Adoptive macrophage directed photodynamic therapy of multidrug-resistant bacterial infection. *Nat Commun.* (2023) 14:7251.
10. Piksa M, Fortuna W, Lian C, Gacka M, Samuel ID, Matczyszyn K, et al. Treatment of antibiotic-resistant bacteria colonizing diabetic foot ulcers by OLED induced antimicrobial photodynamic therapy. *Sci Rep.* (2023) 13:14087.
11. Liu X, Liu S, Mai B, Su X, Guo X, Chang Y, et al. Synergistic gentamicin-photodynamic therapy against resistant bacteria in burn wound infections. *Photodiagn Photodyn Ther.* (2022) 39:103034.
12. Yan E, Kwek G, Qing NS, Lingesh S, Xing B. Antimicrobial photodynamic therapy for the remote eradication of bacteria. *ChemPlusChem.* (2023) 88:e202300009.
13. Mai B, Gao Y, Li M, Wang X, Zhang K, Liu Q, et al. Photodynamic antimicrobial chemotherapy for Staphylococcus aureus and multidrug-resistant bacterial burn infection in vitro and in vivo. *Int J Nanomed.* (2017) 12:5915–31.
14. Naskar A, Kim K-S. Friends against the foe: synergistic photothermal and photodynamic therapy against bacterial infections. *Pharmaceutics.* (2023) 15:1116.
15. Valenzuela-Valderrama M, González IA, Palavecino CE. Photodynamic treatment for multidrug-resistant gram-negative bacteria: perspectives for the treatment of *Klebsiella pneumoniae* infections. *Photodiagn Photodyn Ther.* (2019) 28:256–64.
16. Roa-Tort K, Saavedra Y, Villanueva-Martínez A, Ganem-Rondero A, Pérez-Carranza LA, de la Rosa-Vázquez JM, et al. In vitro antimicrobial photodynamic therapy for *Pseudomonas aeruginosa* (P. aeruginosa) and methicillin-resistant *Staphylococcus aureus* (MRSA) inhibition using a green light source. *Pharmaceutics.* (2024) 16:518.
17. Nie M, Zhang P, Pathak JL, Wang X, Wu Y, Yang J, et al. Photodynamic therapy in periodontitis: a narrative review. *Photodermatol Photoimmunol Photomed.* (2024) 40:e12946.
18. Tichaczek-Goska D, Wojnicz D, Symonowicz K, Ziółkowski P, Hendrich AB. Photodynamic enhancement of the activity of antibiotics used in urinary tract infections. *Lasers Med Sci.* (2019) 34:1547–53.
19. Girigoswami A, Deepika B, Udayakumar S, Janani G, Mercy DJ, Girigoswami K. Peony-shaped zinc oxide nanoflower synthesized via hydrothermal route exhibits promising anticancer and anti-amyloid activity. *BMC Pharmacol Toxicol.* (2024) 25:101.
20. Rajkumar M, Davis Presley S, Thiyagarajulu N, Girigoswami K, Janani G, Kamaraj C, et al. Gelatin/PLA-loaded gold nanocomposites synthesis using *Syzygium cumini* fruit extract and their antioxidant, antibacterial, anti-inflammatory, antidiabetic and anti-Alzheimer's activities. *Sci Rep.* (2025) 15:2110.
21. Calixto GMF, Bernegossi J, De Freitas LM, Fontana CR, Chorilli M. Nanotechnology-based drug delivery systems for photodynamic therapy of cancer: a review. *Molecules.* (2016) 21:342.
22. Sun N, Wen X, Zhang S. Strategies to improve photodynamic therapy efficacy of metal-free semiconducting conjugated polymers. *Int J Nanomed.* (2022) 17:247–71.
23. Salkho NM, Awad NS, Pitt WG, Husseini GA. Photo-induced drug release from polymeric micelles and liposomes: phototriggering mechanisms in drug delivery systems. *Polymers.* (2022) 14:1286.
24. Pawar R, Pathan A, Nagaraj S, Kapare H, Giram P, Wavhale R. Polycaprolactone and its derivatives for drug delivery. *Polymers Adv Technol.* (2023) 34:3296–316.
25. Mohamed RM, Yusoh K. A review on the recent research of polycaprolactone (PCL). *Adv Mater Res.* (2016) 1134:249–55.
26. Dwivedi R, Kumar S, Pandey R, Mahajan A, Nandana D, Katti DS, et al. Polycaprolactone as biomaterial for bone scaffolds: review of literature. *J Oral Biol Craniofac Res.* (2020) 10:381–8.
27. Tay B, Zhang S, Myint M, Ng F, Chandrasekaran M, Tan L. Processing of polycaprolactone porous structure for scaffold development. *J Mater Process Technol.* (2007) 182:117–21.
28. Yadav KS, Sawant KK. Formulation optimization of etoposide loaded PLGA nanoparticles by double factorial design and their evaluation. *Curr Drug Deliv.* (2010) 7:51–64.
29. Piacentini E. Encapsulation efficiency. In: Drioli E, Giorno L editors. *Encyclopedia of Membranes*. Berlin: Springer (2016). p. 706–7.
30. Duse L, Agel MR, Pinnapireddy SR, Schäfer J, Selo MA, Ehrhardt C, et al. Photodynamic therapy of ovarian carcinoma cells with curcumin-loaded biodegradable polymeric nanoparticles. *Pharmaceutics.* (2019) 11:282.
31. Hall BG, Acar H, Nandipati A, Barlow M. Growth rates made easy. *Mol Biol Evol.* (2014) 31:232–8.

32. Kushida Y, Makita Y, Kawakami T, Hoshiko K, Nakagawa H, Nishimura Y, et al. New polymer design by DLS analysis of development defect detection. *J Photopolymer Sci Technol.* (2008) 21:641–6.
33. Marucco A, Aldieri E, Leinardi R, Bergamaschi E, Riganti C, Fenoglio I. Applicability and limitations in the characterization of poly-dispersed engineered nanomaterials in cell media by dynamic light scattering (DLS). *Materials.* (2019) 12:3833.
34. Phillipson K, Hay J, Jenkins M. Thermal analysis FTIR spectroscopy of poly (ε-caprolactone). *Thermochim Acta.* (2014) 595:74–82.
35. Benkaddour A, Jradi K, Robert S, Daneault C. Grafting of polycaprolactone on oxidized nanocelluloses by click chemistry. *Nanomaterials.* (2013) 3:141–57.
36. van Haaren C, De Bock M, Kazarian SG. Advances in ATR-FTIR spectroscopic imaging for the analysis of tablet dissolution and drug release. *Molecules.* (2023) 28:4705.
37. Arbeiter D, Reske T, Teske M, Bajer D, Senz V, Schmitz K-P, et al. Influence of drug incorporation on the physico-chemical properties of poly (L-lactide) implant coating matrices—a systematic study. *Polymers.* (2021) 13:292.
38. Kerimoğlu O, Özer-Önder S, Alarçin E, Karsli S. Formulation and evaluation of the vascular endothelial growth factor loaded polycaprolactone nanoparticles. *Braz J Pharm Sci.* (2022) 58:e19660.
39. Garcez AS, Kaplan M, Jensen GJ, Scheidt FR, Oliveira EM, Suzuki SS. Effects of antimicrobial photodynamic therapy on antibiotic-resistant *Escherichia coli*. *Photodiagn Photodyn Ther.* (2020) 32: 102029.
40. Van Duin D, Paterson D. Multidrug resistant bacteria in the community: trends and lessons learned. *Infect Dis Clin North Am.* (2016) 30: 377.
41. Bharadwaj A, Rastogi A, Pandey S, Gupta S, Sohal JS. Multidrug-resistant bacteria: their mechanism of action and prophylaxis. *BioMed Res Int.* (2022) 2022:5419874.
42. Enright MC, Robinson DA, Randle G, Feil EJ, Grundmann H, Spratt BG. The evolutionary history of methicillin-resistant Staphylococcus aureus (MRSA). *Proc Natl Acad Sci U.S.A.* (2002) 99:7687–92.
43. Vehreschild MJ, Haverkamp M, Biehl LM, Lemmen S, Fätkenheuer G. Vancomycin-resistant enterococci (VRE): a reason to isolate? *Infection.* (2019) 47:7–11.
44. Smith H, Kendall B. *Carbapenem-Resistant Enterobacteriaceae* (CRE). Treasure Islanfe, FL: StatPearls (2019).
45. Kunz Coyne AJ, El Ghali A, Holger D, Rebold N, Rybak MJ. Therapeutic strategies for emerging multidrug-resistant *Pseudomonas aeruginosa*. *Infect Dis Ther.* (2022) 11:661–82.
46. Ibrahim S, Al-Saryi N, Al-Kadmy IM, Aziz SN. Multidrug-resistant *Acinetobacter baumannii* as an emerging concern in hospitals. *Mol Biol Rep.* (2021) 48:6987–98.
47. Feng Y, Tonon CC, Ashraf S, Hasan T. Photodynamic and antibiotic therapy in combination against bacterial infections: efficacy, determinants, mechanisms, and future perspectives. *Adv Drug Deliv Rev.* (2021) 177:113941.
48. Huis in 't Veld RV, Heuts J, Ma S, Cruz LJ, Ossendorp FA, Jager MJ. Current challenges and opportunities of photodynamic therapy against cancer. *Pharmaceutics.* (2023) 15:330.
49. Gunaydin G, Gedik ME, Ayan S. Photodynamic therapy—current limitations and novel approaches. *Front Chem.* (2021) 9:691697.
50. Wang Z, Peng H, Shi W, Gan L, Zhong L, He J, et al. Application of photodynamic therapy in cancer: challenges and advancements. *Biocell.* (2021) 45:489.